Applied Physics Letters

Extreme ultraviolet photoemission of a tin-based photoresist

Cite as: Appl. Phys. Lett. **118**, 171903 (2021); https://doi.org/10.1063/5.0047269
Submitted: 11 February 2021 . Accepted: 12 April 2021 . Published Online: 27 April 2021

Yu Zhang, Jarich Haitjema, Sonia Castellanos, Olivier Lugier, Najmeh Sadegh, Ruslan Ovsyannikov, Erika Giangrisostomi, Fredrik O. L. Johansson, Elin Berggren, Andreas Lindblad, and Albert M. Brouwer

AIP Publishing

Applied Physics Letters ARTICLE scitation.org/journal/apl

Extreme ultraviolet photoemission of a tin-based photoresist

Cite as: Appl. Phys. Lett. **118**, 171903 (2021); doi: 10.1063/5.0047269
Submitted: 11 February 2021 · Accepted: 12 April 2021 ·
Published Online: 27 April 2021

Yu Zhang,[1] Jarich Haitjema,[1] Sonia Castellanos,[1] Olivier Lugier,[1] Najmeh Sadegh,[1] Ruslan Ovsyannikov,[2] Erika Giangrisostomi,[2] Fredrik O. L. Johansson,[3] Elin Berggren,[3] Andreas Lindblad,[3,a)] and Albert M. Brouwer[4,5,a)]

AFFILIATIONS

[1]Advanced Research Center for Nanolithography, Science Park 106, 1098 XG Amsterdam, The Netherlands
[2]Institute Methods and Instrumentation for Synchrotron Radiation Research, Helmholtz-Zentrum Berlin BmbH, Albert-Einstein Straße 15, 12489 Berlin, Germany
[3] X-ray Photon Science, Department of Physics and Astronomy, Uppsala University, Lägerhyddsvägen 1, 75237 Uppsala, Sweden
[4]Advanced Research Center for Nanolithography, Science Park 110, 1098 XG Amsterdam, The Netherlands
[5]University of Amsterdam, van 't Hoff Institute for Molecular Sciences, Science Park 904, 1098 XH Amsterdam, The Netherlands

[a)]**Authors to whom correspondence should be addressed:** andreas.lindblad@physics.uu.se and f.brouwer@arcnl.nl

ABSTRACT

Tin is a suitable element for inclusion in extreme ultraviolet photoresists because of its relatively high-absorption cross section at 92 eV. The electrons emitted after photon absorption are expected to generate secondary electrons in the solid film. In this way, several pathways lead to reactive species that cause a solubility switch. Here, we report the photoelectron spectra of tin oxo cage photoresists over the photon energy range 60–150 eV, and the relative yields of photoelectrons from the valence band of the resist, from the Sn 4*d* orbitals, and of inelastically scattered electrons. The experimental excitation spectra differ considerably from those predicted by commonly used database cross section values, and from the combined computed subshell spectra: the maximum efficiency of ionization of Sn 4*d* both in the photoresists and in Sn metal occurs near the industrially relevant EUV wavelength of 13.5 nm.

Extreme ultraviolet lithography is currently finding its way into industrial application in the semiconductor industry,[1–5] despite the lack of detailed quantitative knowledge about the interaction of the radiation used (92 eV, 13.5 nm) with the materials applied as photoresists. Current implementation of the EUV technology is still based on chemically amplified photoresists, adapted from the well-established ultraviolet lithography that uses laser radiation with a wavelength of 193 nm (6.4 eV).[6,7] Molecular inorganic materials are considered as photoresists for the future because of their higher absorption cross section and potentially high etch resistance.[8–15] The elements with atomic numbers 49 to 54 (In, Sn, Sb, Te, I, and Xe) have large photoionization cross sections at 92 eV that mainly derive from the core level excitation of 4*d* electrons.[16] In order to estimate the photoabsorption and photoemission cross sections of the elements, values from the Centre for X-ray Optics, Berkeley database[17] often reasonably reproduce experimental data,[18–21] especially for the higher photon energies. In this communication, we report our results of a study of metallic tin and tin-based model photoresists (Fig. 1).[22] The latter consist of a cage structure with 12 *n*-butyltin groups bridged by a total of 20 oxygen atoms. Of the *n*-butyltin units, six are in the central "belt" part of the molecule (5-coordinated Sn, black in Fig. 1), and six are on the two equivalent "caps" (6-coordinated, blue). Of the oxygen atoms, twelve are in the central part, six are bridging OH-groups, and two are in the interior of the cage. The tin oxo cage has a net charge of 2+. The three compounds studied differ in the counterions: hydroxide, (TinOH), acetate (TinA), and trifluoroacetate (TinF). We show that the highest yield of Sn 4*d* electrons in the photon energy range 60–150 eV occurs near the EUV energy of 92 eV, rather than near 60 eV, which is predicted by quantum chemical calculations of subshell ionization cross sections.[23] It is commonly accepted that EUV excitation leads to a cascade of secondary electrons, which can induce multiple chemical reactions per photon.[24] The Sn–C bonds in the tin oxo cages are decisively weakened by removing or adding one electron;[15,25–27] the former is the case with the photoionization

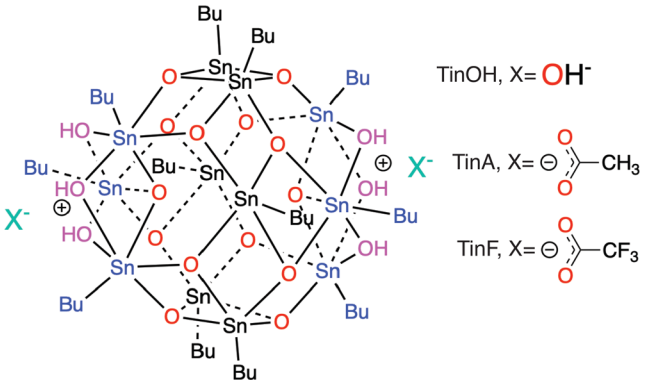

FIG. 1. Molecular structure of the photoresist materials. The *n*-butyltin oxo cage has a 2+ charge, which is compensated by two counterions.

considered herein. The initial kinetic energy distribution after the EUV excitation obtained in the present work is the primary input for modeling the electron cascade and the initiation of chemical conversion in these materials.

Our experiments were performed at the PM4 beam line of BESSY II, using a VG Scienta angle resolved time-of-flight (ArTOF) electron analyzer.[28] The dipole beamline is equipped with a chopper that assures that pulsed x-rays are supplied to the LowDosePES-station. The ArTOF transmission function was measured as a function of electron kinetic energy (see the supplementary material Fig. S1). This was done by fitting the areas of the Au 4*f* photoelectron spectrum from an Au(111) single crystal sample; the spin–orbit components (binding energy 84.00 eV for Au $4f_{7/2}$) were measured in a series of measurements in which the photon energies were varied. The cross section for photoionization of Au 4*f* in this energy range is well known.[29] The variation of photon flux was monitored via a mirror current in the beam line. The additional variation in detected electron intensity arises from the transmission function of the spectrometer. Since different energy windows sample different kinetic energy ranges, two sets of data were measured (using 15% and 5% energy windows).

The experimental Sn 4*d* intensities from the metal were recorded on an argon sputtered piece of polycrystalline Sn/Pb alloy. The Pb 5*d* signal (far from resonance) was used for intensity calibration.

TinOH and TinA were prepared as described previously.[30] TinF was obtained analogously to the synthesis of TinA, by adding two equivalents of trifluoroacetic acid to TinOH in tetrahydrofuran. TinF was characterized by ^{1}H and ^{19}F nuclear magnetic resonance spectroscopy (NMR), see Figs. S5(a) and S5(b). The ^{1}H NMR spectrum is very similar to the spectrum reported (and thoroughly assigned) for TinOH.[31] This result shows that the tin-oxo cage structure has remained completely intact during the conversion of TinOH to TinF. The ^{19}F NMR spectrum confirms that only one type of fluorine atom is present in TinF. Films of tin oxo cages were prepared by spin-coating from toluene solutions on gold-coated silicon as described before.[32] The thickness of the films was ca. 20 nm according to Atomic Force Microscopy measurements.

Molecular structures were optimized using the B3LYP hybrid density functional model with the LANL2DZ effective core potential basis set using Gaussian 16.[33] For more reliable evaluation of (relative) energies, these were calculated using the Def2SVP and Def2TZVP basis sets at the optimized geometries. More details are given in the supplementary material.

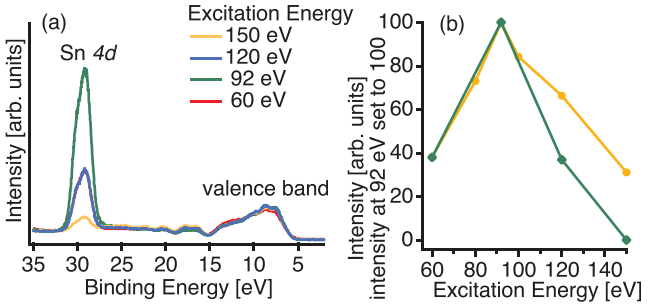

FIG. 2. (a) Photoelectron spectra of a thin film of TinOH at different photon energies. (b) Relative areas of the Sn 4*d* signal spectra of Sn for different photon energies for TinOH (yellow) and Sn reference (green).

The photoelectron spectra obtained for thin films of TinOH spin-coated on gold on silicon are shown in Fig. 2(a). The spectra have been corrected with respect to. spectrometer transmission function. All spectra have been normalized so that the area of the valence band (the energy range 5–15 eV) is set to unity.

To obtain the relative intensity of Sn 4*d* at different excitation energies, the spectra of TinOH were fitted, in a least squares sense, to a series of Voigt functions using the SPANCF routines (written by Kukk) for IGOR PRO (WaveMetrics Inc., Lake Oswego, OR, USA). The goal with the fit was to reproduce the spectral intensity distribution. The Sn 4*d* region was fitted with two components reflecting the spin–orbit splitting of this photoelectron peak. The inelastic losses in the background were modeled by fitting wide peaks to the rising background at the high binding energy side to both the valence and the Sn 4*d* set of lines. The shift between the Sn 4*d* line and the inelastic loss peak was kept the same as the corresponding background to valence band center shift. The results of the fits, including components are presented in the supplementary material, Fig. S3. We find a reasonable agreement between the spectra and the computed orbital energies. The comparison between the computed DOS and the experimental spectrum can be used to identify plasmon components of the experimental spectrum on the high binding energy side (as has been done for other Sn compounds[34,35]). The relative areas of the peak originating from the Sn 4*d* electrons at the different photon energies are given in Table I. The Sn 4*d* signal is dependent on photon energy and is strongest at 92 eV excitation energy. The behavior of the intensity variation in TinOH is similar to that of metallic Sn [see Fig. 2(b)]. As seen in Table I, the size of the inelastic loss background varies relative to that of the main photoelectron signature.

The photoelectron spectra of TinOH are compared with those of TinA and TinF in Fig. 3 for photon energies of 92 eV and 150 eV, respectively.

TABLE I. The size of the Sn 4*d* peak area (26.5 eV–32.3 eV) for different photon energies and the relative size of the inelastic loss background area. See text for details.

$\hbar\omega$ (eV)	60	92	120	150
Sn 4*d* intensity	0.38	1.00	0.37	0.07
Rel. inelastic loss intensity	0.15	0.13	0.09	0.11

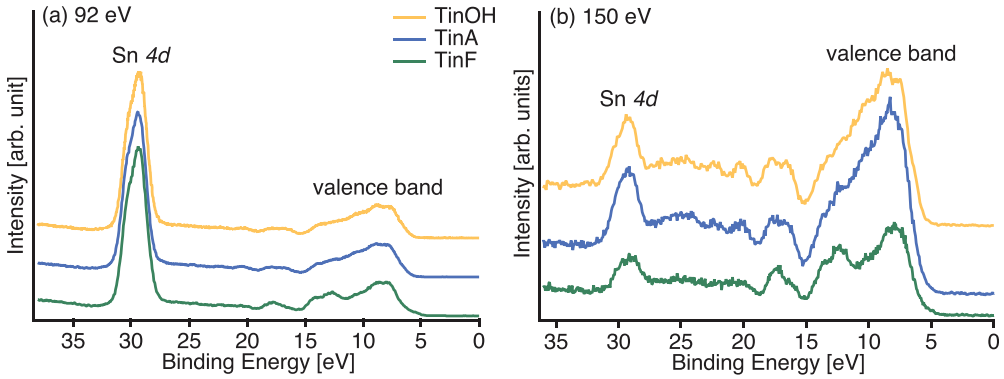

FIG. 3. PES of TinOH, TinAc, and TinF with photon energy (a) 92 eV and (b) 150 eV.

The spectra show a band of valence electrons in the binding energy (BE) range 5–25 eV and Sn 4*d* electrons, which give rise to an unresolved spin–orbit doublet (the split is about 1 eV) near 30 eV. In the gas phase, we found an onset of ionization for the bare dication at 12 eV.[26] This agrees well with the ionization energies calculated (B3LYP/Def2TZVP//LANL2DZ) for the bare dication of 11.9 eV. The value calculated for the neutral TinOH structure is lower because of the electrostatic interaction: 7.2 eV. To approximately account for the interactions with the polarizable environment in the solid, we performed calculations with the Polarizable Continuum Model using diethylether (static dielectric constant 4.24). The interaction further stabilizes the charged species relative to the neutral form, giving a predicted vertical ionization potential (IP) for TinOH of 6.6 eV.

In the thin solid films in the present work, the onset of ionization is found experimentally to agree with that number when the spectra are referenced to the vacuum level. The binding energy scale is constructed using that the ionization potential (IP) is shifted by half the solid's bandgap E_g. (See, e.g., Ref. 36, the Fermi level of an intrinsic semiconductor is approximately in the middle of the bandgap.) Additionally, the work function ϕ (known from calibration) of the system determines the shift between the Fermi level E_F of the solid and the vacuum level. These films are thick enough to safely assume that the interfacial dipole is negligible.[37] The ionization potentials of the molecule and the solid are, thus, related through $IP_{molecule} = IP_{solid} - \phi - E_g/2$. The bandgap of 4.91 eV of the molecular films was obtained from a Tauc-plot (see, e.g., Ref. 38) of the UV/Vis absorption spectrum (see the supplementary material Fig. S2). For the Sn 4*d* electrons of TinOH, the computed orbital energies are ∼−28 eV, in reasonable agreement with the experimental binding energies. The computed density of states is shown in the supplementary material [Figs. S4(a) and S4(b)]. In the energy range 10–25 eV, primary electron emission can occur from C 2*s* (10–20 eV) and O 2*s* orbitals (20–25 eV) (Fig. S4). The spectra of the three tin oxo cages that investigated here do not differ much, as shown in Fig. 3. The calculations suggest that some of the F 2*s* electrons are more strongly bound than Sn 4*d*, but no electrons are detectable in this energy range in Fig. 3(b). In the valence region, the presence of the trifluoroacetate ion gives rise to small extra peaks between 12 eV and 14 eV.

Note that the two different types of Sn atoms in the tin cages are predicted to have slightly different binding energies: the Sn 4*d* electrons of the five-coordinated Sn-atoms in the central belt of the molecule are more strongly bound by 0.6 eV than those of the six-coordinated Sn-atoms at the two caps [see computed DOS in Fig. 4(b)]. This difference together with the spin–orbit splitting of Sn 4*d* of about 1 eV (Table II) is responsible for the broad Sn 4*d* feature.

The Sn 4*d* electrons give rise to two sets of spin–orbit pairs at 29 and 30 eV for all three tin oxo cages studied (see Table II). This binding energy is smaller than values observed for tetramethylstannane $Sn(CH_3)_4$ (30.7 and 31.8 eV,[39] or 31.5 and 32.6 eV[40]). For SnF_2 ca. 2.8 eV, smaller binding energies were found in the solid state than in the gas phase,[41] and if the same difference applies for the tin oxo cages and $Sn(CH_3)_4$, we find that the 4*d* electrons are somewhat more strongly bound in the tin oxo cages than in $Sn(CH_3)_4$. This can be qualitatively explained by the effect of the electronegative oxygen atoms.

The photoionization cross sections for the different subshells were calculated by Yeh and Lindau,[23] and no recent systematic calculations of the same properties are available. The CXRO database contains cross section information based on a combination of experimental and computational data for each element. In Fig. 4(a), we show the predicted cross section for TinOH obtained as a sum of contributions from the different elements (contributions of the different elements are also shown) in the binding energy range between 10

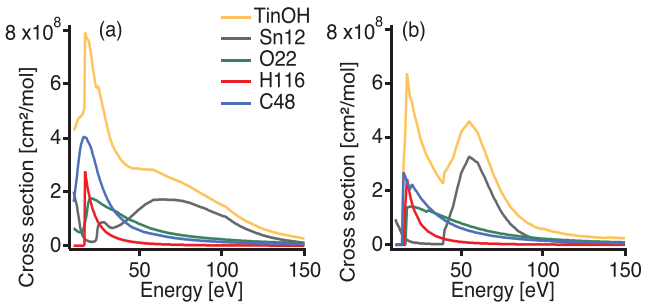

FIG. 4. (a) Cross section of TinOH and the contribution of the different elements to the total from CXRO database[17] and (b) computed cross sections based on the subshell contributions (weighted by the number of atoms) and the total cross section for TinOH as a function of photon energy.[23] Data retrieved from VUO Elettra.[42]

TABLE II. Binding energies recorded at $\hbar\omega = 150$ eV photon energy for Sn 4*d*. See text for details.

	TinOH	TinAc	TinF
E_b [*eV*]	29.1, 30.0	29.0, 30.0	28.9, 29.9

and 200 eV. Figure 4(b) shows the computed subshell contributions (weighted with the number of atoms in the structure).

The cross section near the ionization threshold of Sn 4*d* starting at 28 eV is very small. Only above 45 eV, the computed cross section [Fig. 4(b)] starts to become appreciable, and it peaks near 60 eV. Gas phase studies on tetramethylstannane $Sn(CH_3)_4$[39,40] show a rapid rise of the 4*d* ionization cross section from the onset at 31 eV up to the highest photon energies used in that work, 70 eV. The CXRO data (which include all electrons of each element) show a similar trend, but the decrease in cross section >60 eV is not as drastic as in the computed data [Fig. 4(b)]. Our results show that the maximum in the cross section for Sn 4*d* ionization occurs around 92 eV. A similar discrepancy for 4*d* ionization has been pointed out in the case of CH_3I and its measured 4*d* ionization cross section.[43] This suggest that improved methods are needed for a more accurate computational picture of 4*d* ionization.[16] From a theoretical point-of-view, Cooper and co-workers point out that going beyond the central field approximation and treating electron–electron interaction with more sophistication can shift the maxima of cross sections toward higher kinetic energies.[44]

It is commonly accepted that the chemistry of EUV photoresists is electron-driven.[24,45] After the initial photoionization at 92 eV, the primary electrons emitted from the occupied molecular orbitals have kinetic energies up to 80 eV. These are assumed to initiate a cascade of secondary electrons. When primary electrons are emitted from core levels, such as Sn 4*d*, Auger processes are additional potential sources of electron emission.

Taking the binding energies of about 30 eV for Sn 4*d* and about 5 eV for the HOMO, the Auger electrons can be emitted from orbitals with 5 eV < BE < 15 eV, in which molecular materials are delocalized molecular orbitals (MO). Orbitals that contain important contributions from the atomic orbitals of Sn (5*s* and 5*p*) are at the top of the valence band [Fig. 3(b)]. Although Auger processes probably occur upon excitation at 92 eV, it is difficult to observe them because the emitted electrons have low kinetic energies spread over a broad range since they originate from the valence manifold. For atomic Sn, the NOO Auger spectrum[46] is distributed over kinetic energies <12 eV.

In this communication, we have shown that the orbital origin of the primary photoelectrons in tin oxo cage materials depends strongly on the photon energy. At the technologically relevant photon energy of 92 eV, the ratio of Sn 4d core ionization to valence ionization is particularly large. Thus, both Auger electrons and inelastic processes involving photoelectrons contribute to provide low energy electrons in the system. In this study, we analyze the electron spectrum after excitation, focusing on photoionization cross section and how that may give rise to low energy electrons. This is complementary to studies of the photoabsorption cross section of Sn in the context of EUV lithography.[47]

The present results underscore the usefulness of Sn as a photon absorbing element in EUV photoresists. The ultimate understanding of EUV photochemistry must come from modeling the entire process, from ionization to reactions. Knowledge of the initial electron kinetic energy distribution is a milestone on the (long) road to this understanding.

See the supplementary material for the data, and more detailed descriptions of methods that support the findings of this study.

A part of this work was carried out at ARCNL, a public-private partnership of UvA, VU, NWO, and ASML. A.L. acknowledges the support from the Swedish Research Council (Grant No. 2018-05336). This project has received funding from the European Union's Horizon 2020 research and innovation programme under the Marie Skłodowska-Curie Grant Agreement No. 722149. We thank H.Z.B. for the allocation of synchrotron radiation beamtime (Grant No. 181-06674-ST).

DATA AVAILABILITY

The data that support the findings of this study are available from the corresponding author upon reasonable request.

REFERENCES

[1]A. Lio, "EUV photoresists: A progress report and future prospects," Synchrotron Radiat. News **32**, 9–14 (2019).
[2]E. van Setten, G. Bottiglieri, J. McNamara, J. van Schoot, K. Troost, J. Zekry, T. Fliervoet, S. Hsu, J. Zimmermann, M. Roesch, B. Bilski, and P. Graeupner, "High NA EUV lithography: Next step in EUV imaging," Proc. SPIE **10957**, 1095709 (2019).
[3]N. Fu, Y. Liu, X. Ma, and Z. Chen, "EUV lithography: State-of-the-art review," J. Microelectron. Manuf. **2**, 1–6 (2019).
[4]T. Manouras and P. Argitis, "High sensitivity resists for EUV lithography: A review of material design strategies and performance results," Nanomaterials **10**, 1593 (2020).
[5]C. D. Needham, A. Narasimhan, U. Welling, L. S. Melvin III, P. De Schepper, J. Wouters, J. Severi, D. De Simone, and S. Meyers, "Calibration of a MOx-specific EUV photoresist lithography model," Proc. SPIE **11323**, 113230G (2020).
[6]E. Buitrago, S. Nagahara, O. Yildirim, H. Nakagawa, S. Tagawa, M. Meeuwissen, T. Nagai, T. Naruoka, C. Verspaget, and R. Hoefnagels, "Sensitivity enhancement of chemically amplified resists and performance study using extreme ultraviolet interference lithography," J. Micro/Nanolithogr., MEMS, MOEMS **15**, 033502 (2016).
[7]D. De Simone, Y. Vesters, and G. Vandenberghe, "The path to better understanding stochastics in EUV photoresist," J. Photopolym. Sci. Technol. **31**, 651–655 (2018).
[8]M. Li, V. Manichev, F. Yu, D. Hutchison, M. Nyman, T. Gustafsson, L. C. Feldman, and E. Garfunkel, "Novel Sn-based photoresist for high aspect ratio patterning," Proc. SPIE **10586**, 105860K (2018).
[9]C. Luo, C. Xu, L. Lv, H. Li, X. Huang, and W. Liu, "Review of recent advances in inorganic photoresists," RSC. Adv. **10**, 8385–8395 (2020).
[10]E. C. Mattson, S. M. Rupich, Y. Cabrera, and Y. J. Chabal, "Role of excess ligand and effect of thermal treatment in hybrid inorganic-organic EUV resists," Proc. SPIE **10583**, 1058309 (2018).
[11]S. Castellanos, L. Wu, M. Baljozovic, G. Portale, D. Kazazis, M. Vockenhuber, Y. Ekinci, and T. A. Jung, "Ti, Zr, and Hf-based molecular hybrid materials as EUV photoresists," Proc. SPIE **10583**, 10583A (2018).
[12]H. Xu, V. Kosma, K. Sakai, E. P. Giannelis, and C. K. Ober, "EUV photolithography: Resist progress in metal-organic complex photoresists," J. Micro/Nanolithogr., MEMS, MOEMS **18**, 1 (2018).
[13]R. T. Frederick, S. Saha, J. T. Diulus, F. Luo, J. M. Amador, M. Li, D.-H. Park, E. L. Garfunkel, D. A. Keszler, and G. S. Herman, "Thermal and radiation chemistry of butyltin oxo hydroxo: A model inorganic photoresist," Microelectron. Eng. **205**, 26–31 (2019).

[14]L. Wu, M. Baljozovic, G. Portale, D. Kazazis, M. Vockenhuber, T. Jung, Y. Ekinci, and S. Castellanos, "Mechanistic insights in Zr-and Hf-based molecular hybrid EUV photoresists," J. Micro/Nanolithogr., MEMS, MOEMS **18**, 1 (2019).
[15]I. Bespalov, Y. Zhang, J. Haitjema, R. M. Tromp, S. J. van der Molen, A. M. Brouwer, J. Jobst, and S. Castellanos, "Key role of very low energy electrons in tin-based molecular resists for extreme ultraviolet nanolithography," ACS Appl. Mater. Interfaces **12**, 9881–9889 (2020).
[16]K. D. Closser, D. F. Ogletree, P. Naulleau, and D. Prendergast, "The importance of inner-shell electronic structure for enhancing the EUV absorption of photoresist materials," J. Chem. Phys. **146**, 164106 (2017).
[17]B. Henke, E. Gullikson, and J. Davis, "X-ray interactions-photoabsorption, scattering, transmission and reflection at E = 50–30,000 eV, Z = 1–92," At. Data Nucl. Data Tables **55**, 181–342 (1993).
[18]Y.-J. Kwark, J. P. Bravo-Vasquez, M. Chandhok, H. Cao, H. Deng, E. Gullikson, and C. K. Ober, "Absorbance measurement of polymers at extreme ultraviolet wavelength: Correlation between experimental and theoretical calculations," J. Vac. Sci. Technol. B **24**, 1822–1826 (2006).
[19]R. Fallica, J. K. Stowers, A. Grenville, A. Frommhold, A. P. G. Robinson, and Y. Ekinci, "Dynamic absorption coefficients of chemically amplified resists and nonchemically amplified resists at extreme ultraviolet," J. Micro/Nanolithogr., MEMS, MOEMS **15**, 033506 (2016).
[20]R. Fallica, J. Haitjema, L. Wu, S. Castellanos, A. M. Brouwer, and Y. Ekinci, "Absorption coefficient of metal-containing photoresists in the extreme ultraviolet," J. Micro/Nanolithogr., MEMS, MOEMS **17**, 1 (2018).
[21]N. Sadegh, M. van der Geest, J. Haitjema, F. Campi, S. Castellanos, P. M. Kraus, and A. M. Brouwer, "XUV induced bleaching of a tin oxo cage photoresist studied by high harmonic absorption spectroscopy," J. Photopolym. Sci. Technol. **33**, 145–151 (2020).
[22]B. Cardineau, R. Del Re, M. Marnell, H. Al-Mashat, M. Vockenhuber, Y. Ekinci, C. Sarma, D. A. Freedman, and R. L. Brainard, "Photolithographic properties of tin-oxo clusters using extreme ultraviolet light (13.5 nm)," Microelectron. Eng. **127**, 44–50 (2014).
[23]J. J. Yeh and I. Lindau, "Atomic subshell photoionization cross section and asymmetry parameters: $1 \leq Z \leq 103$," At. Data Nucl. Data Tables **32**, 1–155 (1985).
[24]T. Kozawa and S. Tagawa, "Radiation chemistry in chemically amplified resists," Jpn. J. Appl. Phys., Part 1 **49**, 030001 (2010).
[25]J. Haitjema, Y. Zhang, N. Ottosson, and A. M. Brouwer, "Photoreactions of tin oxo cages, model EUV photoresists," J. Photopolym. Sci. Technol. **30**, 99–102 (2017).
[26]J. Haitjema, L. Wu, A. Guiliani, L. Nahon, S. Castellanos, and A. M. Brouwer, "Photo-induced fragmentation of a tin-oxo cage compound," J. Photopolym. Sci. Technol. **31**, 243–247 (2018).
[27]J. H. Ma, H. Wang, D. Prendergast, A. Neureuther, and P. Naulleau, "Excitation selectivity in model tin-oxo resist: A computational chemistry perspective," Proc. SPIE **11323**, 113231F (2020).
[28]E. Giangrisostomi, R. Ovsyannikov, F. Sorgenfrei, T. Zhang, A. Lindblad, Y. Sassa, U. Cappel, T. Leitner, R. Mitzner, S. Svensson, N. Mårtensson, and A. Föhlisch, "Low dose photoelectron spectroscopy at BESSY II: Electronic structure of matter in its native state," J. Electron Spectrosc. Relat. Phenom. **224**, 68–78 (2018).
[29]L. Johansson, M. Hecht, and I. Lindau, "The energy-dependence of the Au 4f photoionization cross-section," J. Electron Spectrosc. Relat. Phenom. **18**, 271–274 (1980).
[30]J. Haitjema, Y. Zhang, M. Vockenhuber, D. Kazazis, Y. Ekinci, and A. M. Brouwer, "Extreme ultraviolet patterning of tin-oxo cages," J. Micro/Nanolithogr., MEMS, MOEMS **16**, 033510–033517 (2017).
[31]F. Banse, F. Ribot, P. Tolédamo, J. Maquet, and C. Sanchez, "Hydrolysis of monobutylin trialkoxides: Synthesis and characterizations of $((BuSn)_{12}O_{14}(OH)_6)(OH)_2$," Inorg. Chem. **34**, 6371–6379 (1995).
[32]Y. Zhang, J. Haitjema, X. Liu, F. Johansson, A. Lindblad, S. Castellanos, N. Ottosson, and A. M. Brouwer, "Photochemical conversion of tin-oxo cage compounds studied using hard X-ray photoelectron spectroscopy," J. Micro/Nanolithogr., MEMS, MOEMS **16**, 023510–023517 (2017).
[33]M. J. Frisch, G. W. Trucks, H. B. Schlegel, G. E. Scuseria, M. A. Robb, J. R. Cheeseman, G. Scalmani, V. Barone, G. A. Petersson, H. Nakatsuji, X. Li, M. Caricato, A. V. Marenich, J. Bloino, B. G. Janesko, R. Gomperts, B. Mennucci, H. P. Hratchian, J. V. Ortiz, A. F. Izmaylov, J. L. Sonnenberg, D. Williams-Young, F. Ding, F. Lipparini, F. Egidi, J. Goings, B. Peng, A. Petrone, T. Henderson, D. Ranasinghe, V. G. Zakrzewski, J. Gao, N. Rega, G. Zheng, W. Liang, M. Hada, M. Ehara, K. Toyota, R. Fukuda, J. Hasegawa, M. Ishida, T. Nakajima, Y. Honda, O. Kitao, H. Nakai, T. Vreven, K. Throssell, J. A. Montgomery, Jr., J. E. Peralta, F. Ogliaro, M. J. Bearpark, J. J. Heyd, E. N. Brothers, K. N. Kudin, V. N. Staroverov, T. A. Keith, R. Kobayashi, J. Normand, K. Raghavachari, A. P. Rendell, J. C. Burant, S. S. Iyengar, J. Tomasi, M. Cossi, J. M. Millam, M. Klene, C. Adamo, R. Cammi, J. W. Ochterski, R. L. Martin, K. Morokuma, O. Farkas, J. B. Foresman, and D. J. Fox, *Gaussian16 Revision A.03* (Gaussian Inc., Wallingford, CT, 2016).
[34]M. Fondell, M. Gorgoi, M. Boman, and A. Lindblad, "HAXPES study of Sn core levels and their plasmon loss features," Results Phys. **4**, 168–169 (2014).
[35]M. Fondell, M. Gorgoi, M. Boman, and A. Lindblad, "An HAXPES study of Sn, SnS, SnO, and SnO_2," J. Electron Spectrosc. Relat. Phenom. **195**, 195–199 (2014).
[36]H. Peisert, M. Knupfer, and J. Fink, "Energy level alignment at organic/metal interfaces: Dipole and ionization potential," Appl. Phys. Lett. **81**, 2400–2402 (2002).
[37]S. Braun, W. R. Salaneck, and M. Fahlman, "Energy-level alignment at organic/metal and organic/organic interfaces," Adv. Mater. **21**, 1450–1472 (2009).
[38]P. Makuła, M. Pacia, and W. Macyk, "How to correctly determine the band gap energy of modified semiconductor photocatalysts based on UV-Vis spectra," J. Phys. Chem. Lett. **9**, 6814 (2018).
[39]J. Bice, K. Tan, G. Bancroft, and J. Tse, "Variable-energy photoelectron study of the valence levels of $Si(CH_3)_4$ and $Sn(CH_3)_4$ and the tin 4d levels of $Sn(CH_3)_4$," Inorg. Chem. **26**, 4106–4114 (1987).
[40]I. Novak, J. Benson, A. Svensson, and A. Potts, "Photoelectron study of tetramethyl stannane using synchrotron radiation," Chem. Phys. Lett. **135**, 471–474 (1987).
[41]I. Novak and A. W. Potts, "The ultraviolet photoelectron spectra and electronic structure of gas-phase and condensed SnF_2 and PbF_2," J. Chem. Soc., Dalton Trans. **10**, 2211–2213 (1983).
[42]See https://vuo.elettra.eu/services/elements/WebElements.html for "Atomic Calculation of Photoionization Cross-Sections and Asymmetry Parameters" (last accessed June 29, 2020).
[43]T. N. Olney, G. Cooper, and C. Brion, "Quantitative studies of the photoabsorption (4.5–488 eV) and photoionization (9–59.5 eV) of methyl iodide using dipole electron impact techniques," Chem. Phys. **232**, 211–237 (1998).
[44]G. Cooper, J. C. Green, M. P. Payne, B. R. Dobson, and I. H. Hillier, "Photoelectron spectroscopy with variable photon energy. A study of the metal hexacarbonyls M (CO) 6 where M = Cr, Mo, and W," J. Am. Chem. Soc. **109**, 3836–3843 (1987).
[45]R. L. Brainard, M. Neisser, G. Gallatin, and A. Narasimhan, "Photoresists for EUV lithography," in *EUV Lithography*, edited by V. Bakshi (SPIE, 2018), pp. 493–591.
[46]M. Huttula, E. Kukk, S. Heinäsmäki, M. Jurvansuu, S. Fritzsche, H. Aksela, and S. Aksela, "Effects of the open-shell electronic structure in 4d photoionization and Auger decay of atomic Sn," Phys. Rev. A **69**, 012702 (2004).
[47]M. Lysaght, D. Kilbane, N. Murphy, A. Cummings, P. Dunne, and G. O'Sullivan, "Opacity of neutral and low ion stages of Sn at the wavelength 13.5 nm used in extreme-ultraviolet lithography," Phys. Rev. A **72**, 014502 (2005).